QUATERNARY SCIENCE REVIEWS

The International Multidisciplinary Research and Review Journal

Volume 26 Nos 7–8 April 2007 ISSN 0277-3791

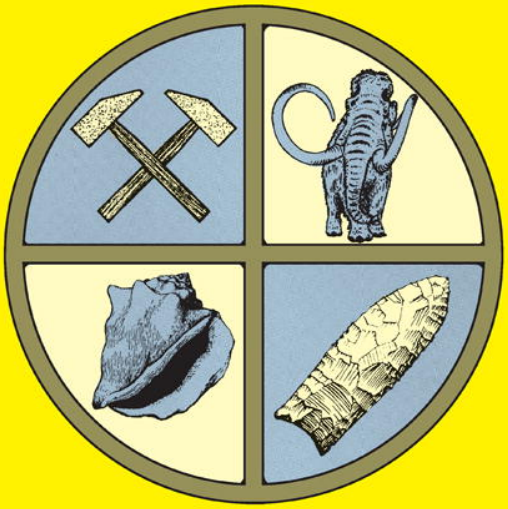

ELSEVIER

Quaternary Science Reviews 26 (2007) 1055–1066

QSR

Cooling of the southern high latitudes during the Medieval Period and its effect on ENSO

Mahyar Mohtadi[a,*], Oscar E. Romero[a], Jérôme Kaiser[b], Dierk Hebbeln[a]

[a]*Center for Marine Environmental Sciences (MARUM), University of Bremen, Germany*
[b]*Geoforschungszentrum (GFZ) Potsdam, Germany*

Received 29 May 2006; received in revised form 6 December 2006; accepted 15 December 2006

Abstract

A high-resolution multiproxy study performed on a marine record from SE Pacific off southern South America was used to reconstruct past regional environmental changes and their relation to global climate, particularly to El Niño/Southern Oscillation (ENSO) phenomenon during the last 2200 years. Our results suggest a sustained northward shift in the position of the zonal systems, i.e. the Southern Westerly Wind belt and the Antarctic Circumpolar Current, which occurred between 1300 and 750 yr BP. The synchrony of the latitudinal shift with cooling in Antarctica and reduced ENSO activity observed in several marine and terrestrial archives across South America suggests a causal link between ENSO and the proposed displacement of the zonal systems. This shift might have acted as a positive feedback to more La Niña-like conditions between 1300 and 750 yr BP by steepening the hemispheric and tropical Pacific zonal sea surface temperature gradient. This scenario further suggests different boundary conditions for ENSO before 1300 and after 750 yr BP.

1. Introduction

The El Niño/Southern Oscillation (ENSO) phenomenon is a natural part of the global climate system that occurs chiefly across its core region in the tropical–subtropical Pacific to Indian Ocean basins (e.g. Allan, 2000). To date, most of the high-resolution marine and terrestrial records dealing with past ENSO variability exist from this "ENSO domain". Rein et al. (2004, 2005) observed a major Holocene El Niño anomaly during the late medieval times (1200–750 yr BP) in a high-resolution flood record off the coast of Peru, and concluded that during some periods, the El Niño activity largely contributes to the global temperature signal, while during others an external forcing is imposed on tropical ENSO. A flood sediment record in a small lake in the Ecuadorian high Andes shows strong ENSO during the 8th and 13th century (1200–1300 and 700–800 yr BP), with weak ENSO activity in between (Moy et al., 2002). These authors attributed the long-term trend to orbitally induced changes in insolation and suggested internal ENSO dynamics as a possible cause of the millennial-scale variability. By studying fossil coral records from Palmyra Island in the central tropical Pacific, Cobb et al. (2003) also suggested that most of the ENSO variability over the last millennium may have arisen from dynamics internal to the ENSO system itself. Their data further imply that the zonal sea surface temperature (SST) gradient across the tropical Pacific could be the key determinant for global climate pattern and may have been steeper before 800 yr BP (Cobb et al., 2003).

As tropical regions are linked to mid- to high latitudes in both hemispheres via teleconnection patterns, any major variation in ENSO is also communicated into more temperate regions (e.g. Philander, 1990). Such ENSO teleconnections and their impact on high latitudes have been the focal point of numerous geophysical studies in the past two decades (e.g. Gu and Philander, 1997; Latif et al., 1997; Montecinos and Aceituno, 2003; Turner, 2004; Yuan, 2004). Among other "footprints" of ENSO, the cryosphere and the atmospheric circulation in the southern

*Corresponding author. Tel.: +49 421 218 65660; fax: +49 421 218 65505.
E-mail address: mohtadi@uni-bremen.de (M. Mohtadi).

0277-3791/$ - see front matter © 2007 Elsevier Ltd. All rights reserved.
doi:10.1016/j.quascirev.2006.12.008

key regions, such as the Ross, Bellingshausen and Weddell seas show a linear relationship to ENSO (e.g. Yuan and Martinson, 2000; Carleton, 2003). In addition, ENSO directly affects the strength and position of the Southern Westerly Wind belt (SWW) and the Antarctic Circumpolar Current (ACC, e.g. Montecinos and Aceituno, 2003; Schneider and Gies, 2004; Turner, 2004). These studies implicate that remote archives from southern high latitudes spanning across a variety of background climate conditions can be used for studying the natural range of ENSO variability and testing the existing ENSO theories and models, and its stable teleconnections.

Here we analyze a high-resolution marine sediment core retrieved off southern South America in the SE Pacific and discuss an additional, possible mechanism for the observed ENSO anomalies during the past two millennia. We further compare our results with prominent high-resolution ENSO archives in order to provide a comprehensive picture of the ENSO signal in the southern hemisphere and to further determine the centennial ENSO variability and its possible forcings and feedbacks.

2. Regional setting

Core GeoB 7186-3 (44° 08.96′S, 75° 09.49′W, water depth 1169 m, length 603 cm) was recovered from the continental slope off Chile, approximately 33 nm west of the northern tip of the Archipelago de Los Chonos, during the RV SO-154 (PUCK) cruise (Hebbeln et al., 2001, Fig. 1). The core position is presently bathed by the poleward-flowing Pacific Deep Water (PDW, >1000 m water depth), overlaid by the equatorward-flowing Antarctic Intermediate Water (AAIW, between ~400 and ~1000 m water depth), and the Subantarctic surface water of the eastward-flowing ACC (Strub et al., 1998).

The ACC transports relatively low saline, cold, phosphate- and nitrate-rich waters originated north of the Subantarctic Front. It deflects into the northward flowing

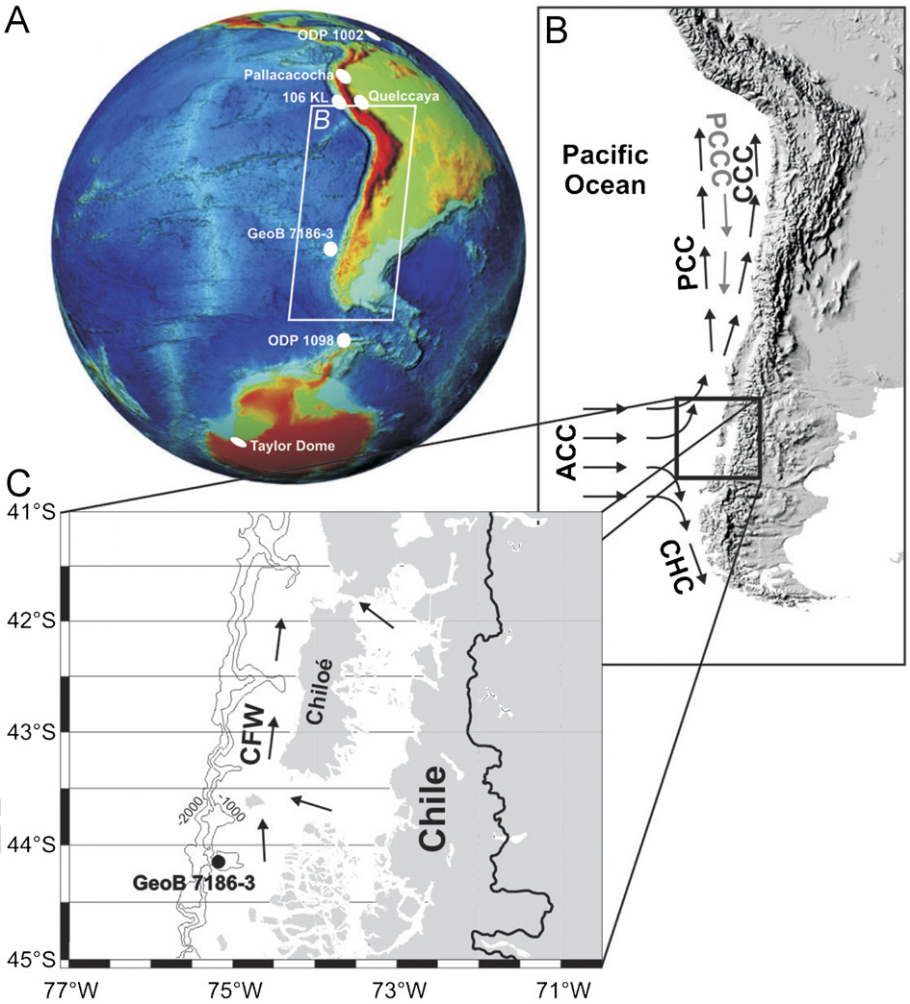

Fig. 1. (A) Position of the investigated core (GeoB 7186-3) and some other high-resolution climate archives discussed in this study (white dots). (B) Schematic map of the present-day general surface circulation pattern in the SE Pacific Ocean. ACC: Antarctic Circumpolar Current, CHC: Cape Horn Current, PCC: Peru–Chile Current, CCC: Chile Coastal Current, PCCC: Peru-Chile Counter Current. (C) Position of the investigated core (black dot) and the main flow direction of the Chilean Fjord Waters (CFW, arrows).

Peru-Chile, or Humboldt, Current (PCC) and the southward flowing Cape Horn Current (CHC) upon reaching the South American continent between ~40°S and 50°S. This area is further characterized by a steep latitudinal SST gradient strongly related to the SWW, and low-salinity surface waters due to the high freshwater supply from the Chilean Fjord Region (CFR, Strub et al., 1998). Based on the salinity fields of Levitus et al. (1994) for off austral Chile between 35°S and 55°S, Dávila et al. (2002) calculated the highest fraction of freshwater in the marine system at 44°S, where core GeoB 7186-3 was retrieved. At the core position, the mean annual SST is presently ~13 °C and varies between 11 °C in winter and 14 °C in summer ⟨http://www.cdc.noaa.gov/⟩; the mean annual sea surface salinity (SSS) resides at ~33‰ (Levitus et al., 1994).

The SWW, the principal precipitation source in the study area, and the associated storm tracks result from the strong thermal gradient and atmospheric pressure difference between cold air masses over Antarctica and warm air masses in the subtropical regions (Cerveny, 1998). Seasonal differences in strength and latitudinal position of the subtropical high pressure and the circum-Antarctic low pressure belt result in the core of the Westerlies to move from ~50°S in austral summer to ~45°S in winter, with an average onshore precipitation of >3000 mm/yr at sea level, and ~1750 mm/yr over the core site (Schneider and Gies, 2004).

The interannual onshore rainfall variability and the SST and SSS in the study area are strongly influenced by ENSO (e.g. Montecinos and Aceituno, 2003; Schneider and Gies, 2004). Rasmusson and Carpenter (1982) showed that precipitation on the Pacific coast of mid-latitude Chile north of 45°S is above average in El Niño years. Cerveny et al. (1987) also found that during periods with negative SOI (El Niño), snow cover between 33°S and 45°S is much more extensive, indicating wetter and colder conditions. However, recent studies show weaker SWW during the El Niño phase of ENSO in southern South America (Turner, 2004). More detailed investigations reveal that during El Niño (La Niña) episodes, typically observed above (below)-average precipitation north of 38°S, and rainfall deficit (excess) between 38°S and 41°S (Montecinos and Aceituno, 2003) and 45°S and 55°S (Schneider and Gies, 2004) are associated with positive (negative) SST anomalies propagating southward along the Chilean coast as far as 37°S (Blanco et al., 2002).

3. Material and methods

3.1. Sampling and stratigraphy

Three sample-series of approx. 10 cm^3 were taken at 5-cm depth intervals from core GeoB 7186-3 for determination of stable oxygen and carbon isotopes, planktonic foraminiferal and diatom composition at an average sample interval of approximately 18 years. The core was sampled for alkenone and opal analyses at depth intervals of 10 cm, with an average temporal resolution of ~35 years. Photospectroscopic and X-ray fluorescence analyses were performed in 1 cm steps corresponding to an average time resolution of ca. 3.6 years. Archived core material is kept at the Department of Geosciences, University of Bremen, Germany.

The age model for core GeoB 7186-3 is based on six ^{14}C accelerator mass spectrometry (AMS) dates (Table 1) and linear interpolation between these dates (Fig. 2). The AMS dates were determined on ca 10 mg carbonate of mixed planktonic foraminifera at the Leibniz laboratory for age determinations and isotope research at the University of Kiel (Nadeau et al., 1997). All ages are corrected for ^{13}C and for a reservoir age of 530 yr based on the calculation by Ingram and Southon (1996) at Puerto Natales, 51°S. The ^{14}C ages were converted into calendar years using the CALPAL software (Jöris and Weninger, 1998, updated 2005) and are reported as years BP ($P = 2000$ AD). The sedimentation rates are in the range of 180–400 cm/ka resulting in an average temporal resolution of ~3.5 yr/cm sediment.

3.2. X-ray fluorescence (XRF) scanning and reflectance spectroscopy

The XRF core scanner is a non-destructive analyses system for relatively fast and closely spaced analyses of major and minor elements by scanning split sediment cores developed at the Netherlands Institute for Sea Research (for further details see Jansen et al., 1998). Iron intensities, used here as a proxy for the terrigenous sediment input, were measured at the Bremen Core Repository on the split cores in 1 cm intervals and are reported as counts per second (cps).

A Gretag Spectrolino (GretagMacbeth, Switzerland) was used onboard to measure the sediment brightness of the split cores in 1 cm intervals immediately after retrieving the core. The split cores were covered with a thin polyethylene transparency to avoid contamination of the sensor head, to protect the sediment from the atmosphere, and to minimize porosity effects. The spectral coverage ranges from 380 to 730 nm, with a spectral resolution of 3 nm band pass filter width which is resampled to 10 nm. A simple ratio of the reflectance at 570 nm over the reflectance at 630 nm provides a proxy for lithics concentrations (Rein and Sirocko, 2002). Further details on the analytical procedure is given in Rein (2003).

3.3. Stable oxygen and carbon isotope measurements

Stable oxygen and carbon isotopes were measured on shells of the planktonic foraminifera species *Neogloboquadrina pachyderma* dex., with a Finnigan MAT 251 mass spectrometer at the isotope laboratory of Department of Geosciences, University of Bremen. Each measurement was performed on 20 individual shells. The isotopic composition of the carbonate sample was measured on

Table 1
Age control points of core GeoB 7186-3

Core depth (cm)	Conventional age (yr BP)	Standard deviation (±yr)	Reservoir age (yr)	CALPAL age (68%) (yr BP)	CALPAL age (2σ, 95%) (yr BP)	CALPAL error (2σ) (±yr)
13	400	25	530	Modern	−40–120	80
108	980	30	530	510	450–570	60
188	1560	25	530	960	920–1000	40
303	1940	45	530	1330	1250–1410	80
408	2290	35	530	1680	1580–1780	100
568	2640	35	530	2080	1980–2180	100

Conventional ages were converted to calendar ages by using CALPAL software (Jöris and Weninger 1998, updated 2005).

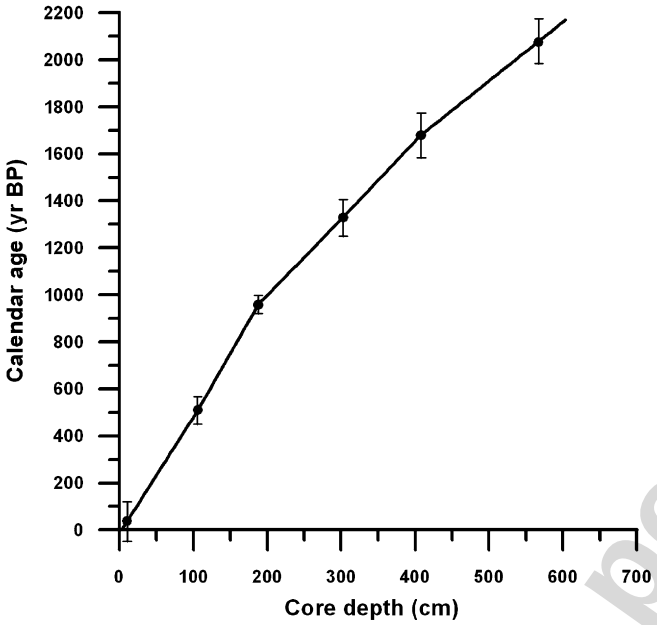

Fig. 2. Age–depth relationship for core GeoB 7186-3 with 2 sigma error bars of the AMS ^{14}C dates (black dots).

the CO_2 gas evolved by treatment with phosphoric acid at a constant temperature of 75 °C. For all stable oxygen isotope measurements a working standard (Burgbrohl CO_2 gas) was used, which has been calibrated against PDB by using the NBS 18, 19 and 20 standards. Consequently, all $\delta^{18}O$ data given here are relative to the PDB standard. Analytical standard deviation is about 0.07‰ for $\delta^{18}O$, and ±0.05 for $\delta^{13}C$ (Isotope Laboratory, Department of Geosciences, University of Bremen).

3.4. Alkenone measurements and SST reconstruction

Alkenones were extracted from 1–3 g of dried and homogenized sediment samples using successively less polar solvent mixtures of methanol (MeOH) and methylene chloride (CH_2Cl_2). As internal standard, 2-nonadecanone ($C_{19}H_{38}O$) was added to the samples prior to extraction. To avoid interferences with co-eluting components, the extracts were saponified. The extracts containing the alkenones were analyzed by capillary gas chromatography using a Hewlett-Packard (HP) 5890 Series II plus gas chromatograph equipped with a DB-5MS fused silica capillary column (60 m, 0.32 mm). We calculated the alkenone unsaturation index from $UK'_{37} = (C_{37:2})/(C_{37:3} + C_{37:2})$, where $C_{37:2}$ and $C_{37:3}$ represent the di- and tri-unsaturated C_{37} alkenones, respectively (Brassell et al., 1986). The UK'_{37} values were converted into temperature values applying the culture calibration of Prahl et al. (1988) ($UK'_{37} = 0.034\,T + 0.039$), which has been validated by core-top compilations (Müller et al., 1998). Based on duplicates and multiple extractions of a sediment sample used as a laboratory-internal reference, the analytical precision (±1σ) was estimated to be of 0.12 °C (0.004 UK'_{37}). Further details on the analytical procedure used for the determination of alkenone SSTs can be found in Kaiser et al. (2005).

3.5. Paleosalinity

The $\delta^{18}O$ composition of planktonic foraminifera ($\delta^{18}O_c$) is controlled by the temperature and the $^{18}O/^{16}O$ ratio of seawater ($\delta^{18}O_{sw}$), which is in turn linearly related to salinity. The combination of the alkenone-based SST results with $\delta^{18}O_c$ data allows reconstructing the $\delta^{18}O_{sw}$ using the paleotemperature (T) equation of Shackleton (1974) [$T = 16.9–4.83*(\delta^{18}O_c–\delta^{18}O_{sw}) + 0.1*(\delta^{18}O_c–\delta^{18}O_{sw})^2$] after the transfer of the $\delta^{18}O_c$ from the PDB to the SMOW unit by adding 0.27‰ to the $\delta^{18}O_c$ values (e.g. Hut, 1987). To estimate the paleosalinity (S; psu) from the $\delta^{18}O_{swcorr}$, the regional $\delta^{18}O_{swcorr}$–salinity relationship for the eastern equatorial Pacific by Fairbanks et al. (1992) [$S = (\delta^{18}O_{sw} + 8.77)/0.26$] was applied, which has a similar slope as modelled by Delaygue et al. (2000) for the Southeast Pacific. Additional effects such as changing isotopic signature of rainfall (Wolff et al., 1998) are unlikely since our study area is situated within the source area of rainfall derived from the SWW.

3.6. Diatom analysis

For the study of siliceous plankton, samples were prepared following the method proposed by Schrader and Gersonde (1978). Qualitative and quantitative analyses were done at ×1000 magnifications using a

Zeiss-Axioscope with phase-contrast illumination. Counts were carried out on permanent slides of acid-cleaned material (Mountex mounting medium). Several traverses across the cover slip were examined, depending on microorganism abundances. At least two cover slips per sample were scanned in this way. Diatom counting of replicate slides indicated that the analytical error of the concentration estimates is $\leqslant 15\%$. The counting procedure and definition of counting units for diatoms to the lowest possible taxonomic level followed those of Schrader and Gersonde (1978).

3.7. Planktonic foraminiferal analyses

The sediment sample set for foraminiferal analyses was freeze-dried, weighed and washed through a 150 μm sieve. At least 300 individuals were individually picked and identified following the taxonomy of planktonic foraminifera proposed by Parker (1962), Kennett and Srinivasan (1983), and Hemleben et al. (1989). For *N. pachyderma* the relative abundances of right (dex.) and left (sin.) coiling individuals were determined, and the two forms were treated as individual species.

4. Results and discussion

Both $\delta^{18}O$ and $\delta^{13}C$ values of the uppermost sample (3 cm, Fig. 3A and E) in core GeoB 7186-3, 0.90 and 1.20‰PDB, match well the surface sediment values that represent the modern benchmark at the same site (7186-1, 0.89 and 1.29‰PDB, Mohtadi et al., 2005) confirming the core top to contain the sediment surface. This finding is supported by the youngest AMS ^{14}C measurement at 13 cm core depth dated younger than AD 1950 (Table 1, Fig. 2).

Warmest SSTs at our core site are recorded prior to ~1300 yr BP, with values around 14 °C (Fig. 3B, black line). A major SST drop of ~1 °C occurred between 1300 and 750 yr BP. The SST shows some fluctuation after 750 yr BP towards the present but remains basically at 13 ± 0.2 °C, except for one outlier (12.3 °C) at 500 yr BP. The SSS record depicts the general SST pattern showing highest values around 36–37‰ before ~1300 yr BP followed by a drop of 1‰ between 1300 and 750 yr BP (Fig. 3B, gray line). The reconstructed SSS shows strong fluctuations from 500 BP towards the present, with relatively higher values around 300 yr BP followed by another significant drop to values of 34–35‰ for the past 200 years.

After Kim et al. (2002), alkenone-based SST estimates closely resemble annual mean temperatures of the surface-mixed layer off Chile. Although the SST reconstruction in this study for the uppermost sample (13.1 °C) matches the modern annual mean SST value (~13 °C, NODC World Ocean Atlas, 1998), the estimated uppermost SSS value (34.8‰) overshoots by far the modern annual mean salinity at the core site (~33.5‰). Our explanation for this discrepancy is that alkenone-derived SST corresponds to the annual average temperature at 0 m water depth, whereas *N. pachyderma* dex., the species used for oxygen isotope measurements, calcifies in deeper depths above the thermocline and, thus, its $\delta^{18}O$ records an average signal through the upper 100 m of the water column (Mohtadi et al., 2005). If we assume 50 m water depth as the mean calcification depth for *N. pachyderma* dex. and correct our uppermost SST value by −1 °C, i.e. the present-day temperature difference between 0 and 50 m water depth at site GeoB 7186-3 (NODC World Ocean Atlas, 1998), the re-calculated uppermost SSS value of 33.6‰ would satisfactorily resemble the present-day salinity at the same depth (~33.6‰, Levitus et al., 1994). In the same manner, all the estimated SSS values downcore would record a rather constant offset of 0.90–0.92‰ and are corrected for 50 m water depth in Fig. 3B. We note that the absolute SSS values are inconsequential for our further considerations since the here discussed SSS pattern remains unaffected.

The ratio of the left-coiling *N. pachyderma* form (N.pas) to the right-coiling form (N.pas/N.pad = N.pas/N.pad + N.pas) shows a continuous baseline shift towards higher values between 1300 and 750 yr BP, followed by decreasing values towards the present (Fig. 3C, black line). Joint relative contribution of *Globigerina bulloides* and *N. pachyderma* sin. to the total planktonic foraminiferal fauna shows the same pattern as for N.pas/N.pad (Fig. 3C, gray line). A vast number of studies suggest that *N. pachyderma* and *G. bulloides* thrive mainly in the well-mixed surface ocean, where phytoplankton density and prey abundance are high (e.g. Sautter and Thunell, 1991; Ortiz et al., 1995; Mohtadi et al., 2005). In addition, some recent studies support the hypothesis that beside the seawater temperature, differences in the adaptation to water mass properties, particularly the stratification of the upper water column, also affect the distribution of the two coiling populations of *N. pachyderma* (Reynolds and Thunell, 1986; Kuroyanagi et al., 2002; Mohtadi et al., 2005). We therefore argue that the comparable patterns of the relative abundances of *G. bulloides* and *N. pachyderma* sin. and N.pas/N.pad reflect the development of the mixed-layer (and thermocline) depth off southern Chile through the past 2200 years.

Shell $\delta^{13}C$ values vary with nutrient concentration and preferred absorption of ^{12}C by photosynthesis at the surface resulting in rather $\delta^{13}C$-enriched surface and $\delta^{13}C$-depleted subsurface waters (Kroopnick, 1985). The $\delta^{13}C$ in the study area is also controlled by mixing of water masses (Lynch-Stieglitz et al., 1994; Mohtadi et al., 2006) due to enhanced air–sea exchange at the surface that leads to $\delta^{13}C$-enriched surface waters (Broecker and Maier-Reimer, 1992). Hence, the observed pattern also reflects the mixing ratio of surface to subsurface waters at the core site (Fig. 3E, gray line).

The Fe intensity as indicator for terrigenous sediment supply and the photospectroscopic proxy for lithics concentration in the sediment show a fairly good overall correlation throughout the core (Fig. 3D). Weak variability in the Fe intensity and lithics concentration within the past

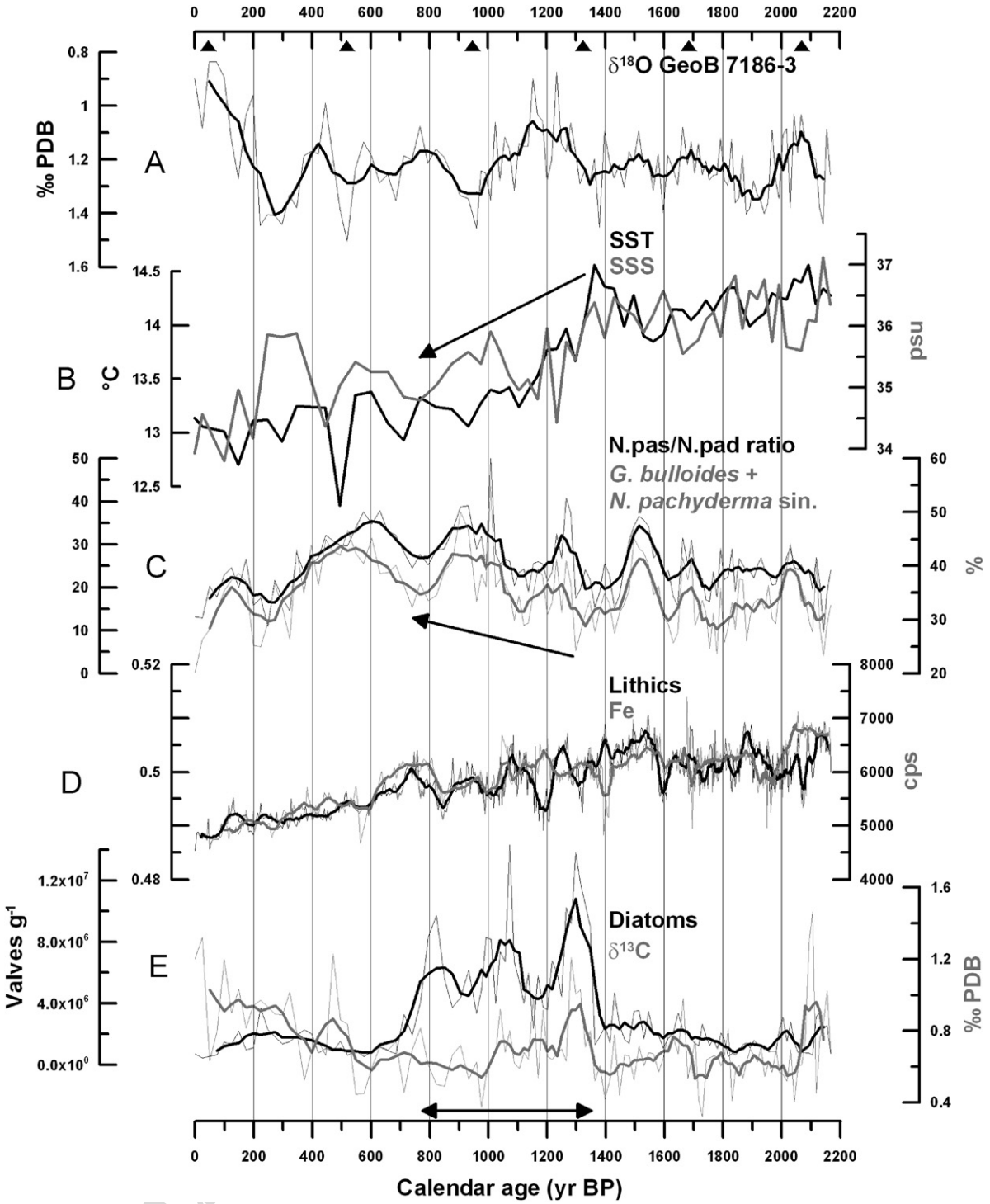

Fig. 3. Results from core GeoB 7186-3. Thick lines represent 5-point running averages, except in D (9-point running average). AMS ^{14}C age control points are indicated with black triangles on top. A: $\delta^{18}O$ record of GeoB 7186-3. (B) Reconstructed (SST, black line) and (SSS, gray line). Note that the SSS values correspond to ~50 m water depth (see text). (C) Ratio between left-coiling *N. pachyderma* and right-coiling *N. pachyderma* (black line), and the joint relative abundances of *N. pachyderma* sin. and *Globigerina bulloides* (gray line). (D) Lithic concentration derived from sediment brightness (black line), and iron intensity in counts per second (gray line). (E) Diatom concentration (black line) and $\delta^{13}C$ of *N. pachyderma* dex. (gray line). Arrows indicate the period of the northward migration of the zonal systems and enhanced productivity.

2200 years reveals negligible changes in the source and composition of the terrigenous material transported to the study area. The smooth decreasing trend in both records towards the present can be attributed to dilution effects as a result of increasing water content in the sediment towards the core top.

Exceptionally high diatom concentrations characterize the period between 1300 and 750 yr BP (Fig. 3E, black

line), with values around one order of magnitude higher than the preceding and following periods. Since the source and composition of the terrigenous input in the study area have not changed significantly during this period, it might be argued that changes in the hydrographic regime at 44°S off Chile account for the observed shift in diatom concentration at our core site. However, we note that variations in the dissolved nutrient content, e.g. in the waters from the CFR, cannot be detected with our terrigenous input proxies.

In the following, we comparatively evaluate the information provided by all the applied proxies in order to understand the climate history off southern Chile and in the SE Pacific for the past 2200 yr. Most significant changes in our multiproxy record within the past 2200 years started at ~1300 yr BP, when the higher-than-present SST and SSS initially dropped towards the present-day values (Fig. 3B), concomitantly with maximum diatom concentration and peak $\delta^{13}C$ values (Fig. 3E). We suggest this was the start of a ~500 year-lasting cooling period associated with the northward migration of the atmospheric and oceanic zonal fronts passing over GeoB 7186-3 at 44°S. At the beginning of this period, an initial atmospheric fingerprint (SWW) of this northward shift can be observed at our core site: enhanced onshore precipitation and input of cold and fresh waters from the CFR with high micronutrient content, mainly dissolved iron, induced SST and SSS drop along with peak diatom concentrations and high $\delta^{13}C$ values. The resulting increased stratification and reduced vertical mixing of the upper water column, recorded in a deep thermocline (Fig. 3C) additionally contributed to the observed high $\delta^{13}C$ values (Fig. 3E, gray line).

During the period between 1300 and 750 yr BP, the shallowing thermocline and enhanced nutrient supply would have favored both the primary (diatom) production and the planktonic foraminiferal species that feed mainly on diatoms under such conditions, i.e. *G. bulloides* and *N. pachyderma* sin. The proposed northward migration of the zonal systems (SWW and ACC) caused a continuous decrease in the SST through the intrusion of colder waters of the ACC, while the SSS decreased mainly through enhanced SWW precipitation at the core site and to some extent also by increased inflow of the Chilean Fjord Waters (CFW). Enhanced freshwater input, however, facilitates the stratification of the upper water column and counteracts the mixing through the front movement, which in turn, appears to be rather a back-and-forth migration than a continual northward shift. The different steps of the northward shift of the zonal systems are best documented in the seesaw pattern of the diatoms and planktonic foraminiferal records along with the strong fluctuation in the SSS record between 1300 and 750 yr BP (Fig. 3B, C and E). Additionally, increased vertical mixing and intrusion of ^{13}C-depleted waters from deeper depths might have accounted for decreasing $\delta^{13}C$ values.

After 600 yr BP, the planktonic foraminiferal records point to gradual deepening of the thermocline towards the present (Fig. 3C). Increasing depth of the thermocline is also indicated by steadily increasing surface water $\delta^{13}C$ values as a result of reduced vertical mixing of the water column (Fig. 3E, gray line). Rather stable SST parallel to generally decreasing but strongly fluctuating SSS are indicative for the effect of river discharge and the CFW at our core site, as under present-day conditions (Dávila et al., 2002), facilitating the stratification of the upper water column and the deepening of the thermocline (Fig. 3B).

Taking together, we propose that over the last 2200 years, the long-term cooling trend observed off southern Chile is linked to the northward shift of the ACC/SWW between 1300 and 750 yr BP. In view of the present-day relation between the seasonal SST variations at site GeoB 7186-3 and the latitudinal migration of the SWW (NODC World Ocean Atlas, 1998, Schneider and Gies, 2004), the 1.1 °C SST decrease between 1300 and 750 yr BP would correspond to ~2° northward displacement of the SSW/ACC. After this period, mixed-layer depth and productivity revert to the conditions prior to the zonal migration. Superimposed to this trend, the observed short-term variability was probably due to changes in the inflow of the relatively fresh, nutrient-rich CFW.

5. Comparison with other southern Hemisphere records

Next we evaluate high-resolution marine and terrestrial records from South America and Antarctica and their adjacent seas spanning the last two millennia in order to examine the possible mechanisms for the observed zonal shift at our core site and its regional and global climatic implications. ODP Site 1002 in Cariaco Basin (Fig. 1A) is supposed to record the mean position of the Inter-Tropical Convergence Zone (ITCZ), with a mean southward (northward) shift of the ITCZ and dry (wet) conditions in northern South America during El Niño (La Niña) events (Haug et al., 2001). Data from the Cariaco Basin show a slight but continuous decrease in precipitation suggestive for a southward migration of the ITCZ before ~1250 yr BP followed by a reversed trend between 1250 and 750 yr BP (Fig. 4A). Decreasing precipitation rates, mirroring the southward shift of the ITCZ and enhanced El Niño events, characterize the period after ~750 yr BP (Haug et al., 2001).

The ice accumulation of the Quelccaya ice cap in Peru (Fig. 1A), indicative for precipitation rates over the Altiplano, abruptly increased at ~1300 yr BP, diminished continuously between 1250 and 750 yr BP, and was followed by a considerable increase between 700 and 400 yr BP (Fig. 4C, Thompson et al., 1985). The primary source for the Andean snowfall is the tropical Atlantic Ocean and hence, the strength of the trade winds controls the observed precipitation pattern in and around the Amazonian Basin and on the Altiplano (Thompson et al., 2000), with warm (cold) and dry (wet) periods during El Niño (La Niña). The two ice accumulation minima at ~1300 and 750 yr BP, therefore, suggest strong ENSO

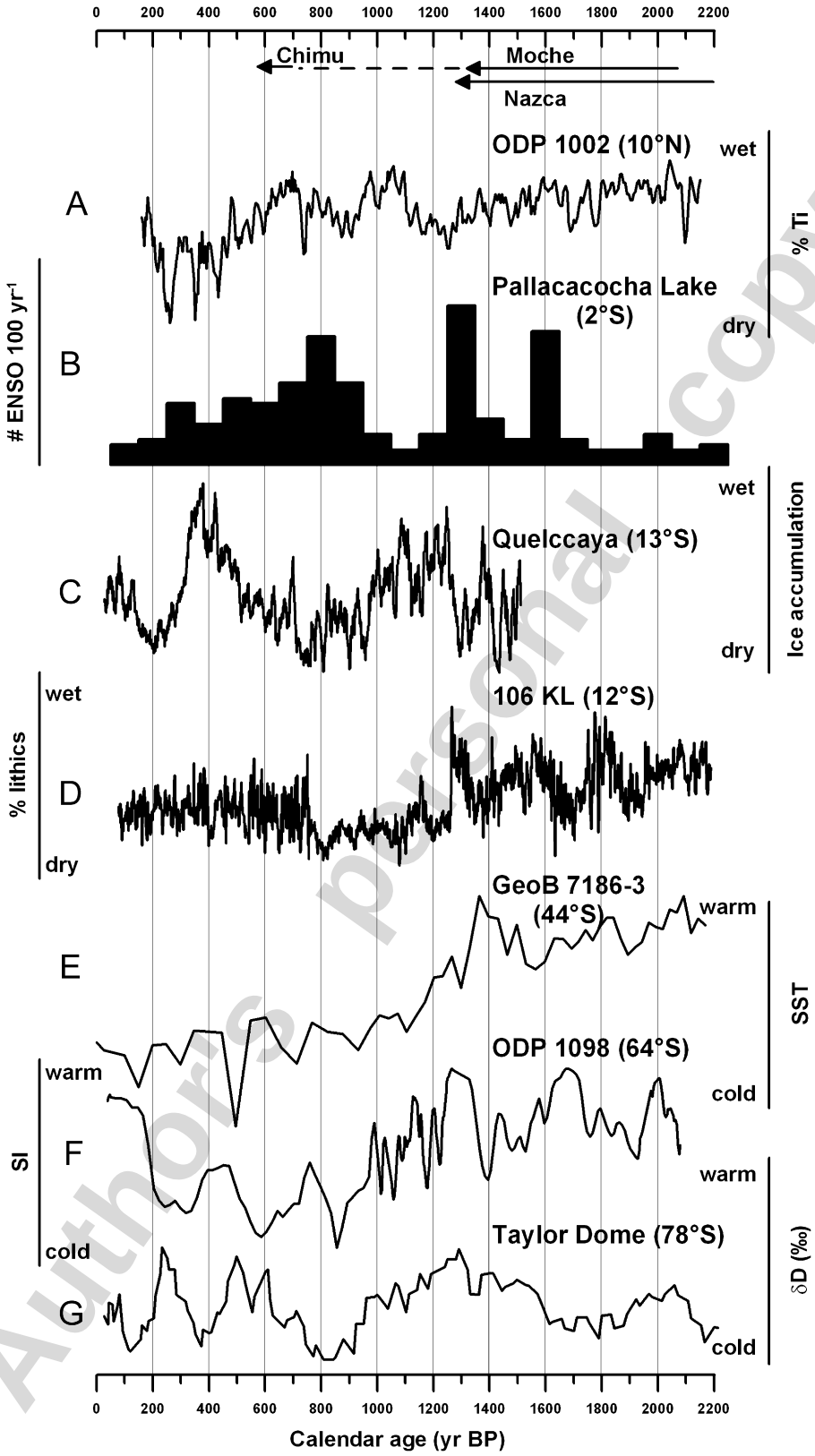

Fig. 4. High-resolution results from climate archives in and around South America and Antarctica. The rise and fall of some ancient Peruvian cultures is indicated with black arrows on top. (A) Titanium record from the Cariaco Basin indicative for precipitation rates and the position of the ITCZ (Haug et al., 2001). (B) El Niño-related flood events from an Ecuadorian lake used to generate an index for the quantity and intensity of ENSO events (Moy et al., 2002). (C) 13-point running average of the ice accumulation in the Quelccaya ice cap (Peru), indicative for the intensity of the trade winds from the tropical Atlantic (Thompson et al., 2000). (D) Lithic concentrations off Peru, used to estimate the Holocene ENSO variability (Rein et al., 2004). (E) SST record of core GeoB 7186-3 (this study). (F) Magnetic susceptibility record from the Palmer Deep reflecting the temperature development off the Antarctic Penninsula (Acton et al., 2001). (G) 9-point running average of the deuterium record in Taylor Dome, Ross Sea (Steig et al., 1998).

events, whereas the maxima at ~1250 and 400 yr BP indicate weak ENSO activities.

Lithic concentrations in core 106 KL taken off Peru has been used to estimate the Holocene climate variability in western South America (Fig. 1A, Rein et al., 2004, 2005). Lowest lithic concentrations between ca 1250 and 750 yr BP have been proposed to reflect the medieval climate anomaly characterized by significantly weaker ENSO activity during this time (Fig. 4D, Rein et al., 2004). This hypothesis is supported by the study of Moy et al. (2002) on El Niño-related flood events from an Ecuadorian lake record (Laguna Pallacacocha, Fig. 1A) showing a maximum of ENSO events around 1300 yr BP followed by minimum occurrence of ENSO events (Fig. 4B). Also a recent study on Palmyra corals implies that the 10th century witnessed the coolest and/or driest conditions in the central tropical Pacific for the last 1100 years (Cobb et al., 2003). Although the relationship between ENSO variance and mean coral $\delta^{18}O$ is weak, the authors suggest less intense ENSO activity between 1100 (oldest dated corals) and ~850 yr BP. The Peruvian drought period proposed from the core 106 KL (Rein et al., 2004) lasted ~100 years longer than the period of minimum ENSO events recorded in the Palmyra corals and Ecuadorian lake sediments (Fig. 4B and D). However, it has to be kept in mind that age discrepancies between marine and terrestrial records as well as between radiometric-dated and continuously-dated paleoclimate records arise from uncertainties in the assumption of reservoir ages, the laboratory dating and calibration errors, and the linearly interpolated age models between calibrated dates. Especially for high-resolution studies, the magnitude of the errors associated with the radiocarbon dating method often hampers a precise correlation between different archives. Furthermore, the ENSO response of distinct archives might vary at different sites (see discussion below in Section 6).

Two large El Niño-driven flood events in south Peru have been dated at A.D. ~700 and A.D. 1300 (1300 and 700 yr BP, Magilligan and Goldstein, 2001). The earlier flood corresponds to peak flood events in Ecuador during the last two millennia (Fig. 4B), highest lithic concentrations in the sediment core off Peru (Fig. 4D), and a southerly position of the ITCZ (Fig. 4A and C), all indicating strong El Niño events. The later flood event marks the end of the proposed Peruvian drought period (Fig. 4D) parallel to the southerly position of the ITCZ (Fig. 4A and C).

The Moche, also Mochica, or the Early Chimu, an ancient narrative civilization known for being prosperous farmers and fishermen, and for their elaborate irrigation canals and aqueducts that brought water for their fields and cities, fell at ~1300 yr BP supposedly due to a 30-yr period of extreme El Niño-related flooding followed by a 30 yr long drought period (for more details see Keatinge, 1988). After a long transition period about which relatively little is known, the Chimu Civilization began at ~800 yr BP in Western Peru, and was characterized by conquest and expansion periods of the late 13th and early 14th century (~700 yr BP). The Nazca, the famous culture that thrived in the southern coastal deserts of Peru with an impressive system of underground aqueducts flourished between 2300 and 1300–1200 yr BP. The contemporaneous fall of strongly rainfall-dependent Nazca and Moche cultures along the Peruvian coast indicates its direct relationship to the observed ENSO anomaly ~1300 yr BP and the subsequent, long-lasting drought period related to weak ENSO activity (Fig. 4, top).

Comparison of the SST record at core GeoB 7186-3 with the magnetic susceptibility record off the Antarctic Peninsula in Palmer Deep (ODP 1098, Acton et al., 2001) and the deuterium record of Taylor Dome (Steig et al., 1998) reveals that the ENSO anomaly at ~1300 yr BP is also witnessed in the southernmost high latitudes (Fig. 4E–G). Relatively high temperatures at 1300 yr BP precede a continuous temperature decrease that lasted until ~850 yr BP at Palmer Deep and Taylor Dome corresponding to the period of the most significant temperature decline at 44°S (Fig. 4E) and minimum ENSO events recorded in Palmyra corals and in the Ecuadorian Lake Pallacacocha (Fig. 4B).

Liu et al. (2002) and Yuan (2004) evaluated the present-day mechanism and impacts of ENSO on southern high latitudes as the most significant teleconnection influencing the high latitude climate modes and their variability (Yuan and Martinson, 2000, 2001). According to these authors, ENSO variability influences the regional Ferrel Cell indirectly by changing the meridional eddy heat flux and shifting the latent heat release zone, which then influences the southern high latitude by modulating the meridional heat flux. Consequentially, warm ENSO events usually generate positive (warm) temperature anomalies and negative (reduced) sea ice anomalies in the Pacific, and an opposite response in the Atlantic center of the so-called "Antarctic Dipole" (ADP, Yuan and Martinson, 2000, 2001). The ADP then evolves and develops its high latitude characteristics in the air–sea–ice coupled system in a different way than the ENSO development (Yuan, 2004). This mechanism satisfactorily explains the observed cooling in the Ross Sea, Palmer Deep and off southern Chile during periods of reduced ENSO that might have caused the northward shift of the SWW (ACC) in (off) southern South America and the ITCZ in northern South America between 1300 and ~750 yr BP. The correlation among these records is, however, poor for the remaining periods, especially after ~750 yr BP. Obviously, other factors have been affecting or modulating the response of the different climate archives to ENSO events, or their teleconnections, prior to 1300 yr BP and after ~750 yr BP (see discussion below).

6. Possible forcings and internal dynamics

Assuming that the temperature patterns in South America and Central and East Pacific mirror changes in

the ENSO intensity, several questions arise regarding the forcing and the mechanisms responsible for its regional and global propagation. What did trigger the extremely high number of ENSO events at ~1300 yr BP (~30, Fig. 4B, Moy et al., 2002), especially in light of the small changes in the solar activity for the last 2000 years (Stuiver et al., 1998)? Why did the proxies responded only to this and the following period of weak ENSO activity until ~750 yr BP, and why is this evidence restricted to these records and Palmyra corals, although several studies suggest ENSO to be presently the major source of global interannual climate variability (Philander, 1990) with robust atmospheric teleconnections (e.g. Latif et al., 1997)?

The growth and decay of ENSO is best explained with a Pacific recharge oscillator including the relationship between the equatorial western Pacific thermocline depth and the eastern Pacific SST anomalies (Jin, 1997). The intensity, frequency and mode of ENSO can change through time (see Diaz and Markgraf, 2000) and cause sustained and long-lasting effects on the hydrological regime within its realm: a coral record from the Galapagos Islands implies that the vertical thermal structure of the eastern tropical Pacific changed in 1976, and that the increase in the frequency and intensity of El Niño events since then might be a result of the deepening of the eastern tropical Pacific thermocline (Guilderson and Schrag, 1998). In the same manner, the ENSO behavior between 1300 and 800 yr BP can be explained in terms of variability in the upwelling intensity and thermocline depth in the eastern equatorial Pacific: strong ENSO events at ~1300 yr BP precede a sustained northward displacement of the zonal systems towards their present-day location in the SE Pacific, as indicated in our record, probably triggering strong La Niña-like conditions between 1300 and ~800 yr BP. This northward shift of ~2° of latitude would have steepened the hemispheric thermal gradient with stronger meridional and zonal winds resulting in thermocline shoaling in the eastern tropical Pacific and steepened tropical Pacific E–W temperature gradient acting as a positive feedback triggering more La Niña-like conditions (less ENSO activity) in the following centuries. This scenario can also be observed in the present-day propagation of the ENSO signal with resulting changes in the location and variability of the SWW/ACC, although the relationship is highly non-linear and even breaks down in some years (see review by Turner, 2004). The inception of more intense ENSO activities at the end of this period at 800–700 yr BP occurred under changed boundary conditions compared to before 1300 yr BP, i.e. under the modern position of the SSW/ACC and a shallower eastern tropical Pacific thermocline. This hypothesis is best supported by the records presented in Fig. 4, all indicating different environmental conditions before and after the period between 1300 and 750 yr BP.

It is beyond the scope of this study to determine whether the strong ENSO events at 1300 and 750 yr BP were generated by the ocean thermostat (Clement et al., 1996), higher solar activity around 1400 and 800 yr BP (Stuiver et al., 1998), or strong volcanic eruptions (Adams et al., 2003), e.g. the El Chichón eruption at AD 1259 (741 yr BP, Langway et al., 1995), or a combination of these forcings. Kreutz et al. (1997) suggested that the meridional atmospheric circulation intensity in the polar South Pacific and the North Atlantic abruptly increased at ~600 yr BP, with enhanced precipitation in California and Patagonia (Stine, 1994) without any direct connection to insolation. These dates (1300, 750 and 600 yr BP) mark the onset of the MWP, the first (Wolf) and the second (Spörer) sunspot minima within the LIA, respectively. From these data it appears that little changes in the solar forcing and/or the tropical SST are capable of triggering a large extra-tropical response, as indicated in our record at ~1300 yr BP. Nonlinear ocean–atmosphere interactions, as e.g. sea ice extension in the southern high latitudes and equatorward displacement of the zonal systems may have amplified solar forcing and acted as positive feedback on the tropical Pacific climate (Clement et al., 1999).

Stronger fluctuations in solar activity would serve as an explanation for the observed discrepancy between remote archives on multi-decadal/centennial scale after ~750 yr BP, when external forcing modulates the global climate and the signal of internal climate dynamics, as e.g. the ENSO signal, might be suppressed or even absent in some remote archives. However, Rein et al. (2005) showed that correlation between El Niño activity and global temperature exists in part within the last millennium, although solar activity was highly variable. An alternative explanation for the weak or varying ENSO responses in the South American records after 750 yr BP could be the change in the ENSO variance after 750 yr BP, as recorded in the Palmyra corals, probably due to the changed boundary conditions caused by, or associated with, a more northerly position of the SWW/ACC. As proposed for the period between 1300 and 750 yr BP, the potential for changes in ENSO characteristics without a significant external trigger allows for a nonlinear response of the global climate to linear forcing in the future and therefore holds significant implications for future climate changes.

7. Conclusions

1. Our data suggest a 2° northward shift of the SWW/ACC between 1300 and 750 yr BP. This shift caused the SST and SSS decrease at 44°S in the SE Pacific towards their modern values.
2. We suggest that the zonal fronts passing over the core site enhanced sporadically the primary production (diatoms) by favouring a shallowing thermocline and enhanced nutrient supply (dissolved iron) from the continent.
3. From the proxy data it appears that ENSO has been operating under different conditions since ~750 yr BP. This change started ~550 years earlier, following the strong ENSO anomaly at ~1300 yr BP.

4. Different boundary conditions for ENSO might be causally linked to the changed position of the zonal systems modifying the thermocline depth in the eastern tropical Pacific.

Acknowledgments

We thank M. Segl, B. Meyer-Schack, R. Kreutz and M. Buëmann for performing lab work. This study was supported by the German Bundesministerium für Bildung und Forschung through funding of the project "PUCK" (03G0156A). The Research Center Ocean Margins at the University of Bremen provided technical support. F. Lamy and another anonymous reviewer provided useful comments to the manuscript. The data presented in this study are also available in digital format at 〈www.pangaea.de.〉 This is a RCOM publication no.. RCOM0448.

References

Acton, G.D., Borton, C.J., The Leg 178 Shipboard Scientific Party, 2001. Palmer Deep composite depth scales for Leg 178 Sites 1098 and 1099, In: Baker, P.F., Camerlenghi, A., Acton, G.D., Ramsay, A.T.S. (Eds.), Proceedings of the ODP, Sci. Results, 178 [Online], 〈http://www-odp.tamu.edu/publications/178_SR/chap_05/chap_05.htm〉

Adams, B.J., Mann, M.E., Ammann, C.M., 2003. Proxy evidence for an El Niño-like response to volcanic forcing. Nature 426, 274–278.

Allan, R.J., 2000. ENSO and climate variability in the past 150 years. In: Diaz, H.F., Markgraf, V. (Eds.), El Niño and the Southern Oscillation: Multi Scale Variability and Global and Regional Impacts. Cambridge University Press, Cambridge, pp. 3–57.

Blanco, J.L., Carr, M.E., Thomas, A.C., Strub, P.T., 2002. Hydrographic conditions off northern Chile during the 1996–1998 La Niña and El Niño events. Journal of Geophysical Research—Oceans 107.

Brassell, S.C., Eglinton, G., Marlowe, I.T., Pflaumann, U., Sarnthein, M., 1986. Molecular stratigraphy: a new tool for climatic assessment. Nature 320, 129–133.

Broecker, W.S., Maier-Reimer, E., 1992. The influence of air and sea exchange on the carbon isotope distribution in the sea. Global Biogeochemical Cycles 6, 315–320.

Carleton, A.M., 2003. Atmospheric teleconnections involving the Southern Ocean. Journal of Geophysical Research 108 (C4), 8080.

Cerveny, R.S., 1998. Present climates of South America. In: Hobbs, J.E., Lindesay, J.A., Bridgman, H.A. (Eds.), Climates of the Southern Continents: Present, Past and Future. Wiley, New York, pp. 107–134.

Cerveny, R.S., Skeeter, B.R., Dewey, K.F., 1987. A preliminary investigation of a relationship between South American snow cover and the southern oscillation. Monthly Weather Review 115, 620–623.

Clement, A.C., Seager, R., Cane, M.A., Zebiak, S.E., 1996. An ocean dynamical thermostat. Journal of Climate 9, 2190–2196.

Clement, A.C., Seager, R., Cane, M.A., 1999. Orbital controls on the El Niño/Southern Oscillation and the tropical climate. Paleoceanography 14, 441–456.

Cobb, K.M., Charles, C.D., Cheng, H., Edwards, R.L., 2003. El Niño/Southern Oscillation and tropical Pacific climate during the last millennium. Nature 424, 271–276.

Dávila, P.M., Figueroa, D., Müller, E., 2002. Freshwater input into the coastal ocean and its relation with the salinity distribution off Austral Chile (35–55°S). Continental Shelf Research 22, 521–534.

Delaygue, G., Jouzel, J., Dutay, J.-C., 2000. Oxygen 18-salinity relationship simulated by an oceanic general circulation model. Earth and Planetary Science Letters 178, 113–123.

Diaz, H.F., Markgraf, V., 2000. El Niño and the Southern Oscillation. Cambridge University Press, Cambridge, p. 512.

Fairbanks, R.G., Charles, C.D., Wright, J.D., 1992. Origin of global meltwater spikes. In: Taylor, R.E. (Ed.), Radiocarbon After Four Decades. Springer, New York, pp. 473–500.

Gu, D., Philander, S.G.H., 1997. Interdecadal climate fluctuations that depend on exchanges between the tropics and extratropics. Science 275, 805–807.

Guilderson, T.P., Schrag, D.P., 1998. Abrupt shift in subsurface temperatures in the tropical pacific associated with changes in El Niño. Science 281, 240–243.

Haug, G.H., Hughen, K.A., Sigman, D.M., Peterson, L.C., Röhl, U., 2001. Southward migration of the intertropical convergence zone through the holocene. Science 293, 1304–1308.

Hebbeln, D., et al., 2001. PUCK, Report and Preliminary Results of R/V Sonne Cruise SO 156, Valparaiso (Chile)—Talcahuano (Chile), March 29–May 14, 2001, Berichte aus dem Fachbereich Geowissenschaften 182, Universität Bremen, p. 195.

Hemleben, C., Spindler, M., Anderson, O.R., 1989. Modern Planktonic Foraminifera. Springer, New York, pp. 363.

Hut, G., 1987. Consultants Group Meeting on Stable Isotopic Reference Samples for Geochemical and Hydrological Investigations. International Atomic Energy Agency, Vienna, p. 42.

Ingram, B.L., Southon, J.R., 1996. Reservoir ages in Eastern Pacific coastal and estuarine waters. Radiocarbon 38, 573–582.

Jansen, J.H.F., Van der Gaast, S.J., Koster, B., Vaars, A.J., 1998. CORTEX, a shipboard XRF-scanner for element analyses in split sediment cores. Marine Geology 151, 143–153.

Jin, F.-F., 1997. An Equatorial Ocean recharge paradigm for ENSO. Part I: conceptual model. Journal of the Atmospheric Sciences 54, 811–829.

Jöris, O., Weninger, B., 1998. Extension of the ^{14}C calibration curve to ca 40,000 cal BC by synchronizing Greenland $^{18}O/^{16}O$ ice core records and North Atlantic foraminifera profiles: a comparison with U/Th coral data. Radiocarbon 40, 495–504.

Kaiser, J., Lamy, F., Hebbeln, D., 2005. A 70-ka sea surface temperature record off southern Chile (Ocean Drilling Programm Site 1233). Paleoceanography 20, PA4009.

Keatinge, R.W., 1988. Peruvian Prehistory: An Overview of Pre-Inca and Inca Society. Cambridge University Press, Cambridge.

Kennett, J.P., Srinivasan, M., 1983. Neogene Planktonic Foraminifera—A Phylogenetic Atlas. Hutchinson Ross Publishing, Stroudsburg, p. 265.

Kim, J., Schneider, R.R., Hebbeln, D., Müller, P.J., Wefer, G., 2002. Last deglacial sea–surface temperature evolution in the southeast Pacific compared to climate changes on the South American continent. Quaternary Science Reviews 21, 2085–2097.

Kreutz, K.J., Mayewski, P.A., Meeker, L.D., Twickler, M.S., Whitlow, S.I., Pittalwala, I.I., 1997. Bipolar changes in atmospheric circulation during the Little Ice Age. Science 277, 1294–1296.

Kroopnick, P., 1985. The distribution of ^{13}C of ΣCO_2 in the world oceans. Deep-Sea Research 32, 57–84.

Kuroyanagi, A., Kawahata, H., Nishi, H., Honda, M.C., 2002. Seasonal changes in planktonic foraminifera in the northwestern North Pacific Ocean: sediment trap experiments from subarctic and subtropical gyres. Deep Sea Research Part II 49, 5627–5645.

Langway Jr., C.C., Osada, K., Clausen, H.B., Hammer, C.U., Shoji, H., 1995. A 10-century comparison of prominent bipolar volcanic events in ice cores. Journal of Geophysical Research 100, 16241–16248.

Latif, M., Kleeman, R., Eckert, C., 1997. Greenhouse warming, decadal variability, or El Niño? An attempt to understand the anomalous 1990s. Journal of Climate 10, 2221–2239.

Levitus, S., Burgett, R., Boyer, T.B., 1994. World Ocean Atlas, vol. 3: Salinity. US Department of Commerce, Washington, DC, p. 99.

Liu, J., Yuan, X., Rind, D., Martinson, D.G., 2002. Mechanism study of the ENSO and southern high latitude climate teleconnections. Geophysical Research Letters 29, 1.

Lynch-Stieglitz, J., Fairbanks, R.G., Charles, C.D., 1994. Glacial–interglacial history of Antarctic Intermediate Water: relative strengths of Antarctic versus Indian Ocean sources. Paleoceanography 9, 7–29.

Magilligan, F.J., Goldstein, P.S., 2001. El Nino floods and culture change: a late Holocene flood history for the Rio Moquegua, southern Peru. Geology 29, 431–434.

Mohtadi, M., Hebbeln, D., Marchant, M., 2005. Upwelling and productivity along the Peru–Chile Current derived from faunal and isotopic compositions of planktic foraminifera in surface sediments. Marine Geology 216, 107–126.

Mohtadi, M., Hebbeln, D., Nuñez-Ricardo, S., Lange, C.B., 2006. El Niño-like pattern in the Pacific during Marine Isotope Stages (MIS) 13 and 11? Paleoceanography 21, PA1015.

Montecinos, A., Aceituno, P., 2003. Seasonality of the ENSO-related rainfall variability in central Chile and associated circulation anomalies. Journal of Climate 16, 281–296.

Moy, C.M., Seltzer, G.O., Rodbell, D.T., Anderson, D.M., 2002. Variability of El Nino/Southern Oscillation activity at millennial timescales during the Holocene epoch. Nature 420, 162–165.

Müller, P.J., Kirst, G., Ruhland, G., von Storch, I., Rosell-Melé, A., 1998. Calibration of the alkenone paleotemperature index UK′37 based on core tops from the eastern South Atlantic and the global ocean (60°N–60°S). Geochimica et Cosmochimica Acta 62, 1757–1772.

Nadeau, M.J., Schleicher, M., Grootes, P.M., Erlenkeuser, H., Gottolong, A., Mous, D.J.W., Sarnthein, J.M., Willkomm, N., 1997. The Leibniz-Labor AMS facility at the Christian-Albrechts University, Kiel, Germany. Nuclear Instruments and Methods in Physics Research 123, 22–30.

Ortiz, J.D., Mix, A.C., Collier, R.W., 1995. Environmental control of living symbiotic and asymbiotic foraminifera of the California Current. Paleoceanography 10, 987–1009.

Parker, F., 1962. Planktic foraminifera species in Pacific sediments. Micropaleontology 8, 219–254.

Philander, S.G.H., 1990. El Niño, La Niña and the Southern Oscillation. Elsevier, New York, p. 293.

Prahl, F.G., Muehhausen, L.A., Zahnle, D.L., 1988. Further evaluation of long-chain alkenones as indicators of paleoceanographic conditions. Geochimica et Cosmochimica Acta 52, 2303–2310.

Rasmusson, E.M., Carpenter, T.H., 1982. Variation in tropical sea surface temperature and surface wind fields associated with the El Niño-southern oscillation. Monthly Weather Review 110, 354–384.

Rein, B., 2003. *In-Situ* Reflektionsspektroskopie und digitale Bildanalyse: Gewinnung hochauflösender Paläoumweltdaten mit fernerkundlichen Methoden. habilitation thesis, University of Mainz, Mainz, Germany, 104 pp.

Rein, B., Sirocko, F., 2002. *In-situ* reflectance spectroscopy—analysing techniques for high-resolution pigment logging in sediment cores. International Journal of Earth Sciences 91, 950–954.

Rein, B., Lückge, A., Sirocko, F., 2004. A major Holocene ENSO anomaly during the Medieval period. Geophysical Research Letters 31, L17211.

Rein, B., Lückge, A., Reinhardt, L., Sirocko, F., Wolf, A., Dullo, W.C., 2005. El Niño variability off Peru during the last 20,000 years. Paleoceanography 20, PA4003.

Reynolds, L.A., Thunell, R.C., 1986. Seasonal production and morphologic variation of *Neogloboquadrina pachyderma* (Ehrenberg) in the northeast Pacific. Micropaleontology 32, 1–18.

Sautter, L.R., Thunell, R.C., 1991. Planktonic foraminiferal response to upwelling and seasonal hydrographic conditions: sediment trap results from San Pedro Basin, Southern California. Journal of Foraminiferal Research 21, 347–363.

Schneider, C., Gies, D., 2004. Effects of El Niño-Southern Oscillation on southernmost South America precipitation at 53°S revealed from NCEP–NCAR reanalyses and weather station data. International Journal of Climatology 24, 1057–1076.

Schrader, H., Gersonde, R., 1978. Diatoms and silicoflagellates. In: Zachariasse, W.J., Riedel, W.R., Sanfilippo, A., Schmidt, R.R., Brolsma, M.J., Schrader, H., Gersonde, R., Drooger, M.M., Broekman, J.A. (Eds.), Micropaleontological Counting Methods and Techniques—An Exercise on an Eight Meter Section of the Lower Pliocene of Capo Rosello, Sicily. Ultrecht Micropaleontology Bulletin, pp. 129–176.

Shackleton, N., 1974. Attainment of isotopic equilibrium between ocean water and the benthonic foraminifera genus *Uvigerina*: isotopic changes in the ocean during the last glacial. In: Labeyrie, L. (Ed.), Les méthodes quantitatives d'étude des variations du climat au cours du Pléistocène. CNRS, Paris, pp. 203–209.

Steig, E.J., Brook, E.J., White, J.W.C., Sucher, C.M., Bender, M.L., Lehman, S.J., Morse, D.L., Waddington, E.D., Clow, G.D., 1998. Synchronous climate changes in Antarctica and the North Atlantic. Science 282, 92–95.

Stine, S., 1994. Extreme and persistent drought in California and Patagonia during mediaeval time. Nature 369, 546–549.

Strub, P.T., Mesías, J.M., Montecino, V., Rutllant, J., Salinas, S., 1998. Coastal ocean circulation off western South America. In: Robinson, A.R., Brink, K.H. (Eds.), The Global Coastal Ocean—Regional Studies and Synthesis. The Sea, Ideas and Observations on Progress in the Study of the Seas. Wiley, New York, pp. 273–313.

Stuiver, M., Reimer, P.J., Bard, E., Beck, W., Burr, G.S., Hughen, K.A., Kromer, B., McCormac, G., van der Plicht, J., Spurk, M., 1998. INTCAL98 radiocarbon age calibration, 24,000-0 cal BP. Radiocarbon 40, 1041–1083.

Thompson, L.G., Mosley-Thompson, E., Bolzan, J.F., Koci, B.R., 1985. A 1500 year record of tropical precipitation recorded in ice cores from the Quelccaya Ice Cap, Peru. Science 229, 971–973.

Thompson, L.G., Henderson, K.A., Mosley-Thompson, E., Lin, P.N., 2000. The tropical ice core record of ENSO. In: Diaz, H.F., Markgraf, V. (Eds.), El Niño and the Southern Oscillation: Multiscale Variability and Global and Regional Impacts. Cambridge University Press, Cambridge, pp. 325–357.

Turner, J., 2004. The El Niño-southern oscillation and Antarctica. International Journal of Climatology 24, 1–31.

Wolff, T., Mulitza, S., Arz, H., Pätzold, J., Wefer, G., 1998. Oxygen isotopes versus CLIMAP (18 ka) temperatures: a comparison from the tropical Atlantic. Geology 26, 675–678.

Yuan, X., 2004. ENSO-related impacts on Antarctic sea ice: a synthesis of phenomenon and mechanisms. Antarctic Science 16, 415–425.

Yuan, X., Martinson, D.G., 2000. Antarctic sea ice extent variability and its global connectivity. Journal of Climate 13, 1697–1717.

Yuan, X., Martinson, D.G., 2001. The Antarctic dipole and its predictability. Geophysical Research Letters 28, 3609–3612.